

# Calcination effects on the crystal structure and magnetic properties of $\text{CoFe}_2\text{O}_4$ nanopowders synthesized by the coprecipitation method

G. Márquez<sup>a,\*</sup>, V. Sagredo<sup>a</sup>, R. Guillén-Guillén<sup>a</sup>, G. Attolini<sup>b</sup>, and F. Bolzoni<sup>b</sup>

<sup>a</sup>*Departamento de Física, Universidad de Los Andes,  
5101 Mérida, Venezuela.*

*\*e-mail: gersonmarquez@ula.ve*

<sup>b</sup>*Istituto dei Materiali per l'Elettronica ed il Magnetismo, Consiglio Nazionale delle Ricerche  
Parco Area delle Scienze 37 A, 43124 Parma, Italy.*

Received 16 May 2019; accepted 6 January 2020

Cobalt ferrite nanopowders were successfully synthesized by the coprecipitation method and subsequent calcination at 873 and 1073 K. The effects of the thermal treatments on the crystal structure, particle size and magnetic properties of the nano-compounds were investigated. The particle sizes were determined from transmission electron microscopy, and an increase in sizes with the increment in calcination temperature was observed. The mean particle sizes were 29 and 42 nm, for samples calcined at 873, and 1073 K, respectively. By X-ray diffraction, it was determined that the nanoparticles crystallized in the cubic spinel structure. Additionally, Fourier transform infrared spectroscopy studies confirm the presence of spinel metal oxide. The magnetization measurements as a function of the temperature and the applied magnetic field suggested that a large part of the nanoparticles calcined at 873 K present a superparamagnetic behavior at room temperature, while those calcined at 1073 K are mainly in the blocked regime at temperatures below 320 K. Besides remarkably high coercivities of approximately 10.7 and 12.4 kOe were observed at low temperatures, for the nanopowders calcined at 873 and 1073 K, respectively.

**Keywords:** Cobalt ferrite; nanostructured materials; coprecipitation; crystal structure; magnetization.

PACS: 61.46.Df; 75.50.Tt; 81.07.Wx.

DOI: <https://doi.org/10.31349/RevMexFis.66.251>

## 1. Introduction

Ferrites are a class of metal oxides with remarkable physical properties, being the most studied ferrimagnetic materials, since the 1940s [1,2]. During the last  $\sim 60$  years, ferrites have been used in many technological applications ranging from simple permanent magnets to magnetic recording, magnetic storage, and medical applications such as: hyperthermia, magnetic resonance imaging, and drug delivery [3-6].

The ferrites with formula unit  $\text{AFe}_2\text{O}_4$  (where A are divalent cations such as:  $\text{Mn}^{2+}$ ,  $\text{Fe}^{2+}$ ,  $\text{Co}^{2+}$ , and  $\text{Ni}^{2+}$ ) crystallizes in the well known cubic spinel structure, in which the  $\text{A}^{2+}$  and  $\text{Fe}^{3+}$  cations are located in interstices with tetrahedral and octahedral coordination. The cation distribution between the tetrahedral and octahedral sites occurs in two types of structural arrangements, known as normal spinel and inverse spinel. In the normal spinel, the  $\text{A}^{2+}$  cations are located in the tetrahedral sites, while the  $\text{Fe}^{3+}$  cations are in the octahedral interstices. On the other hand, in the inverse spinel, one-half of the  $\text{Fe}^{3+}$  cations are located in the tetrahedral sites and the other half of the trivalent cations, together with all the  $\text{A}^{2+}$  cations, are located in the octahedral interstices. However, there are many possible intermediate cation distributions represented by  $(\text{A}_{1-\lambda}\text{B}_\lambda)^T(\text{A}_\lambda\text{B}_{2-\lambda})^O\text{O}_4$ , where  $\lambda$  is called inversion parameter, and  $T$  and  $O$  superscripts indicate the tetrahedral and octahedral positions, respectively. These last cation distributions are known as partially inverse spinels [3,7]. Cation distribution depends on different factors, such as the cation radii, thermal history, and particle size. The cation distribution in partially inverse spinels is sen-

sitive to thermal treatments, and the synthesis method used [8]. Cobalt ferrite ( $\text{CoFe}_2\text{O}_4$ ) is a partially inverse spinel, and  $0.62 \leq \lambda \leq 0.93$  was reported for this ferrite [9]. Bulk cobalt ferrite is a ferrimagnet at room temperature, with a Curie temperature of  $\sim 790$  K [10].  $\text{CoFe}_2\text{O}_4$  nanoparticles have been extensively investigated, because of its high coercivity, high magnetocrystalline anisotropy, and its moderate saturation magnetization [7].

In the synthesis of cobalt ferrite nanoparticles, various methods have been used, such as: coprecipitation [11-13], sol-gel [14,15], combustion reaction [16,17], micro-emulsion [18], hydrolysis reaction [19], high-temperature decomposition of organic precursors [20], polymer pyrolysis [21]. Among them, coprecipitation is one of the most used, due to it's a very simple, fast, and low-cost method [22].

A nanopowder is made up of an aggregation of nanoparticles, which change their characteristics according to the synthesis method used and/or type of drying. A as-synthesized nanopowder commonly presents traces of by-products of the synthesis process; therefore, it is appropriate to perform thermal treatments to the dried material. These heat treatments or calcinations allow obtaining nanopowders cleaner, with higher crystallinity and nanoparticles of larger sizes [23,24].

In the present investigation, cobalt ferrite nanopowders have been synthesized by the coprecipitation method, using metal nitrates and ammonium hydroxide. We report on the crystal structure, size, and magnetic properties of  $\text{CoFe}_2\text{O}_4$  nanoparticles, calcined at 873 and 1073 K.

## 2. Experimental

### 2.1. Synthesis of nanopowders

Cobalt ferrite nanoparticles were synthesized by the coprecipitation method, following the synthesis procedure described below: stoichiometric amounts of cobalt nitrate ( $\text{Co}(\text{NO}_3)_2 \cdot 6\text{H}_2\text{O}$ ) and ferric nitrate ( $\text{Fe}(\text{NO}_3)_3 \cdot 9\text{H}_2\text{O}$ ), for 2 g of final compound, were dissolved in 100 ml of deionized water at room temperature and stirred for 15 min continuously by magnetic stirring. Then, maintaining constant stirring, 100 ml of ammonium hydroxide solution ( $\text{NH}_4\text{OH}$ , 29.66 wt% in water) was added, initially dropwise to destabilize the precursor solution and start the precipitation of the compound, and immediately the rest in excess to get a solution with basic pH about 12. Then, the solution was stirred vigorously and constantly at room temperature, for 1 hour; The resulting solution-precipitate was dried in an oven at 373 K, for 48 hours, until obtaining the as-synthesized nano-compound.

Later on, to study the influence of the thermal treatment on the crystal structure, size, and magnetic properties of nanoparticles, the as-synthesized compound was divided into two samples, which were calcined in a furnace with an air atmosphere, at 873 and 1073 K, during 2 hours. The heating rate from room temperature to the calcination temperatures was  $1^\circ\text{C}/\text{min}$ . After calcination, the samples were naturally cooled in the air down to room temperature.

### 2.2. Characterization techniques

X-ray powder diffraction (XRD) data of the synthesized nanopowders has been recorded in a Philips diffractometer, using  $\text{CuK}\alpha$  radiation in the  $2\theta$  range from  $15$  to  $70^\circ$ , to characterize the crystal structure of the nanoparticles. To know the chemical composition of the nano-compounds, Fourier transform infrared (FTIR) spectra were acquired using a PerkinElmer FTIR spectrophotometer, between  $4000$  and  $380\text{ cm}^{-1}$ , on sample pellets prepared dispersing the ferrite powders at 1.5% in potassium bromide (KBr). Micrographs of the nanopowders were taken employing a JEOL JEM 1220 transmission electron microscope (TEM), to determine the particle sizes, and explore the morphology and aggregation of nanoparticles in the samples. For the observation in the microscope, a drop of diluted suspension of nanoparticles in ethanol was placed on a carbon-coated copper grid. The particle size distribution was evaluated by measuring the largest dimension of at least 150 nanoparticles. Subsequently, the size histograms were adjusted to a Log-normal distribution, obtaining the mean particle sizes. Magnetization measurements were performed by using a SQUID magnetometer. The temperature dependence of the magnetization was measured with 10 Oe applied field, in zero-field-cooled (ZFC) and field-cooled (FC) modes, between 5 and 320 K. Hysteresis loops were obtained by applying a magnetic field up to 55 kOe, at two temperatures: 5, and 320 K.

## 3. Results and discussion

### 3.1. X-ray diffraction studies

X-ray diffractograms of the nanopowders calcined at 873 and 1073 K are presented in Fig. 1. Both diffractograms exhibit only diffraction peaks corresponding to the standard XRD pattern of the cobalt ferrite (JCPDS: 22-1086), which indicates that a single crystalline phase corresponding to the cubic spinel structure was obtained in the two powder samples. Comparing the two XRD patterns, it is observed that the diffraction peaks of the calcinated sample at 1073 K are narrower and more intense, which suggests that it improves the crystallinity and increase the particle sizes with the increment of the calcination temperature. The unit cell parameter ( $a$ ) was determined using the Le Bail refinement method. The X-ray density ( $\rho_{\text{x-ray}}$ ) was calculated using the relation  $\rho_{\text{x-ray}} = 8M/N \cdot a^3$ , where  $M$  is the molecular weight of the compound,  $N$  is Avogadro's number, and  $a$  is the lattice parameter. The theoretical bulk density ( $\rho_{\text{th}}$ ) was determined from sample pellets, using the equation  $\rho_{\text{th}} = m/\pi r^2 h$ , where  $m$  is the mass,  $r$  is the radius, and  $h$  is the height of the pellet. The porosity ( $P$ ) of the two samples was calculated using the relation  $P = ((\rho_{\text{x-ray}} - \rho_{\text{th}})/\rho_{\text{x-ray}}) \cdot 100\%$  [25]. The values of  $a$ ,  $\rho_{\text{x-ray}}$ ,  $\rho_{\text{th}}$ , and  $P$  are tabulated in Table I. It is observed that the unit cell parameter increases from  $8.343\text{ \AA}$ , in Co ferrite calcined to 873 K, to  $8.362\text{ \AA}$  in the sample calcined to 1073 K, which indicates that there is a slight expansion of the lattice with the increase of the calcination temperature. The  $\rho_{\text{th}}$  and  $P$  values suggest that densification occurs, in addition to a samples' porosity reduction with the increase in calcination temperature. These results confirm that the applied thermal treatments generate sintering of the nanoparticles, as has been reported in other studies [24,25].

### 3.2. Infrared spectroscopy studies

Figure 2 shows the FTIR spectra of the two samples of cobalt ferrite nanoparticles in KBr, where absorption bands are ob-

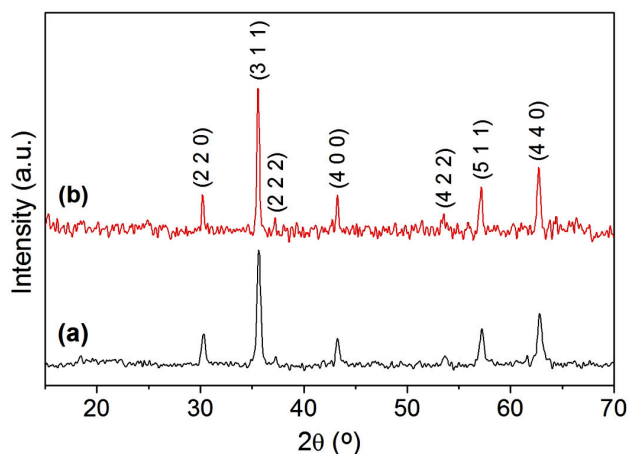


FIGURE 1. X-ray diffractograms of cobalt ferrite nanopowders calcined at (a) 873 K and (b) 1073 K.

TABLE I. Particle size ( $D$ ), unit cell parameter ( $a$ ), X-ray density ( $\rho_{x\text{-ray}}$ ), theoretical bulk density ( $\rho_{\text{th}}$ ), and porosity ( $P$ ) of cobalt ferrite nanoparticles calcined at 873 and 1073 K.

Sample	$D$ (nm)	$a$ (Å)	$\rho_{x\text{-ray}}$ (g/cm <sup>3</sup> )	$\rho_{\text{th}}$ (g/cm <sup>3</sup> )	$P$ (%)
Calcined at 873 K	29	8.343 (1)	5.367	3.749	30.15
Calcined at 1073 K	42	8.362 (4)	5.331	4.182	21.55

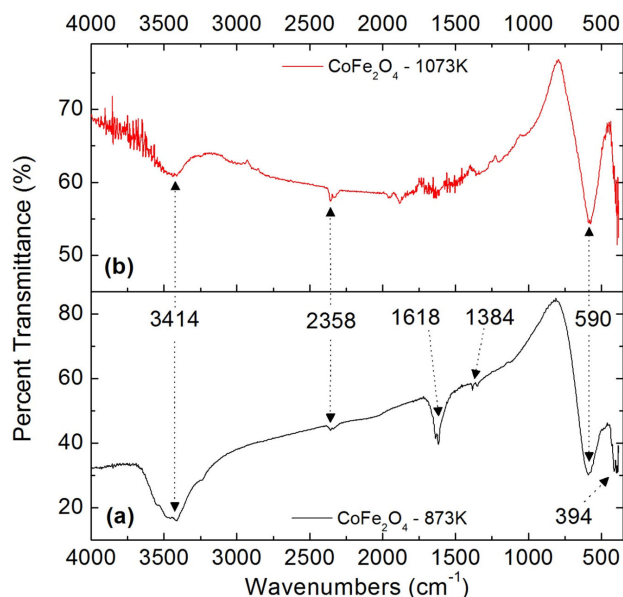
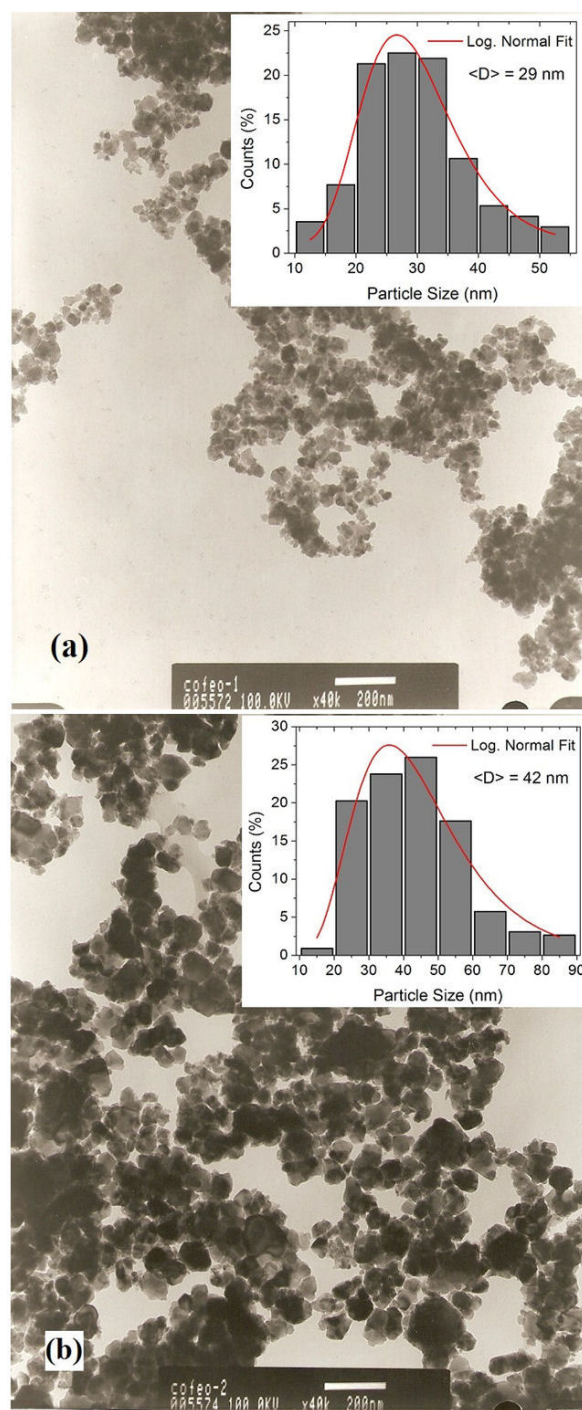


FIGURE 2. FTIR spectra of cobalt ferrite nanoparticles calcined at (a) 873 K and (b) 1073 K.

served at 3414, 2358, 1618, 1384, 590, and 394 cm<sup>-1</sup>. The first absorption bands are assigned as follows: 3414 cm<sup>-1</sup> corresponds to vibrations of O-H bonds, 2358 and 1618 cm<sup>-1</sup> are due to N-H vibrations, and 1384 cm<sup>-1</sup> is associated with vibrations of N-O bonds. Therefore, these first vibrational bands reveal the presence of impurity molecules such as adsorbed water, amines, ammonium ions, and nitro compounds, which are by-products derived from the reagents used in the synthesis of nanopowders. The last two absorption bands are produced by the metal-oxygen vibrations of the ferrite. These vibrational bands correspond to two of the four vibrations active in the infrared, as predicted by the group theory for crystals with spinel structure [26]. The  $\nu_1$  band observed at 590 cm<sup>-1</sup> is due to the vibration of the ions located in the tetrahedral coordination sites of the spinel structure, while  $\nu_2 = 394$  cm<sup>-1</sup> is attributed to the vibration of the ions in octahedral positions [26,27]. Therefore, these two absorption bands assigned to the Co-O and Fe-O stretching correspond to the fingerprint of the cobalt ferrite, confirming the formation of the cubic spinel crystalline phase in the synthesized nanopowders. Comparing the FTIR spectra of the two samples, it is observed that the absorption bands associated with impurities in the nano-compound calcined at 1073 K are less intense than those in the sample calcined at 873 K, which indicates that with the increase in the calcina-

FIGURE 3. TEM images and size histograms of CoFe<sub>2</sub>O<sub>4</sub> nanoparticles calcined at (a) 873 K and (b) 1073 K.

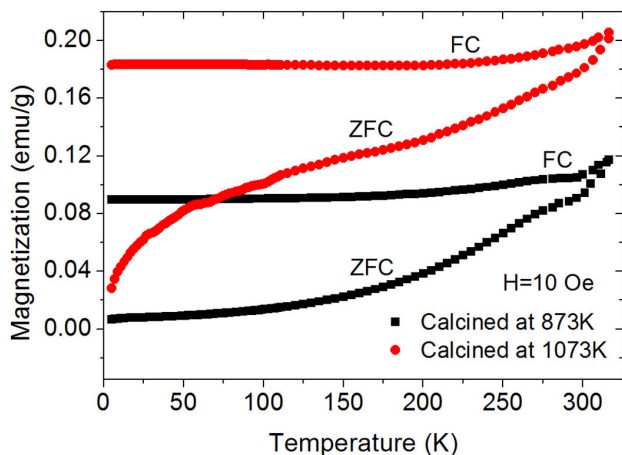


FIGURE 4. Temperature dependence of the ZFC and FC magnetization of  $\text{CoFe}_2\text{O}_4$  nanoparticles calcined at 873 and 1073 K.

tion temperature, it is possible to obtain cleaner nanopowders. On the contrary, the vibrational bands  $\nu_1$  and  $\nu_2$  are more pronounced in the sample calcined at 1073 K, confirming that the crystallinity of the nanoparticles improves with the increase in the calcination temperature, in accordance with the results obtained from the X-ray diffraction study.

### 3.3. Transmission electron microscopy studies

Figure 3 shows the TEM images of both samples of  $\text{CoFe}_2\text{O}_4$ , in addition to the respective size histograms. Comparing the two micrographs taken at the same magnification ( $\times 40\text{k}$ ), it is evident that the size of the nanoparticles increased with the increment in the calcination temperature. It can be noticed a significant agglomeration of nanoparticles with irregular shapes. The histograms reveal that the two nano-compounds have wide size distributions, with nanoparticle sizes ranging from approximately 12 to 53 nm (for the sample calcined at 873 K), and from 15 to 85 nm (for the sample calcined at 1073 K). Therefore, increasing the calcination temperature increased the particle sizes dispersion. The Log-normal fits of the size distributions allowed to obtain mean particle sizes of 29, and 42 nm, for the samples calcined at 873 and 1073 K, respectively.

### 3.4. Magnetic studies

Figure 4 shows the temperature dependence of the magnetization, in ZFC and FC conditions, for the two cobalt ferrite samples. In both ZFC-FC magnetization curves, irreversibility between 5 and 320 K is observed, suggesting the coexistence of superparamagnetic nanoparticles together with a non-negligible fraction of nanoparticles still in the blocked regime, at room temperature. The TEM study reveals that practically all the synthesized nanoparticles are smaller than the known critical single domain size for Co ferrite (70 nm) [6]. Therefore, both  $\text{CoFe}_2\text{O}_4$  samples may have a predominantly superparamagnetic behavior at room temperature. The non-overlap of the ZFC-FC curves at 320 K

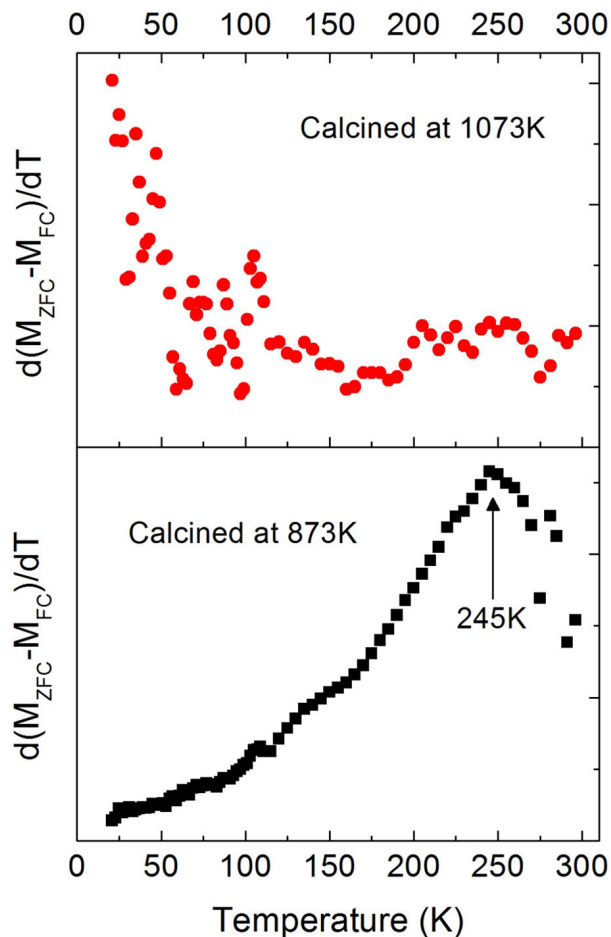


FIGURE 5. the Derivative of  $M_{ZFC} - M_{FC}$  concerning to temperature, as a function of temperature, for  $\text{CoFe}_2\text{O}_4$  nanoparticles calcined at 873 and 1073 K.

can be due to the wide size distributions with large mean particle sizes, but also to the presence of strong interparticle interactions. In Fig. 4 it can be noted that the FC magnetization data does not increase as usually does in a non-interacting nanoparticle system. This decrease of FC magnetizations with the lowering temperature is indicative of the presence of strong magnetic interactions between the nanoparticles in the two nanopowder samples [28]. Additionally, it is also observed that the ZFC-FC magnetization data of the sample calcined at 1073 K are greater than those of the sample calcined at 873 K, which is attributed to the increase in the magnetic nanoparticle sizes with the increment in the temperature of the applied thermal treatment.

The blocking temperature distributions for the two  $\text{CoFe}_2\text{O}_4$  samples are shown in Fig. 5. These curves were obtained from the derivative  $d(M_{ZFC} - M_{FC})/dT$ , where  $M_{ZFC}$  and  $M_{FC}$  are the ZFC and FC magnetizations, respectively. In the curve of the sample calcined at 873 K, a maximum is observed at  $T = 245$  K, which corresponds to the representative blocking temperature ( $T_B$ ) of this nanopowder. On the other hand, in the  $T_B$  distribution of the sample calcined at 1073 K, there is no maximum attributable to the average

value

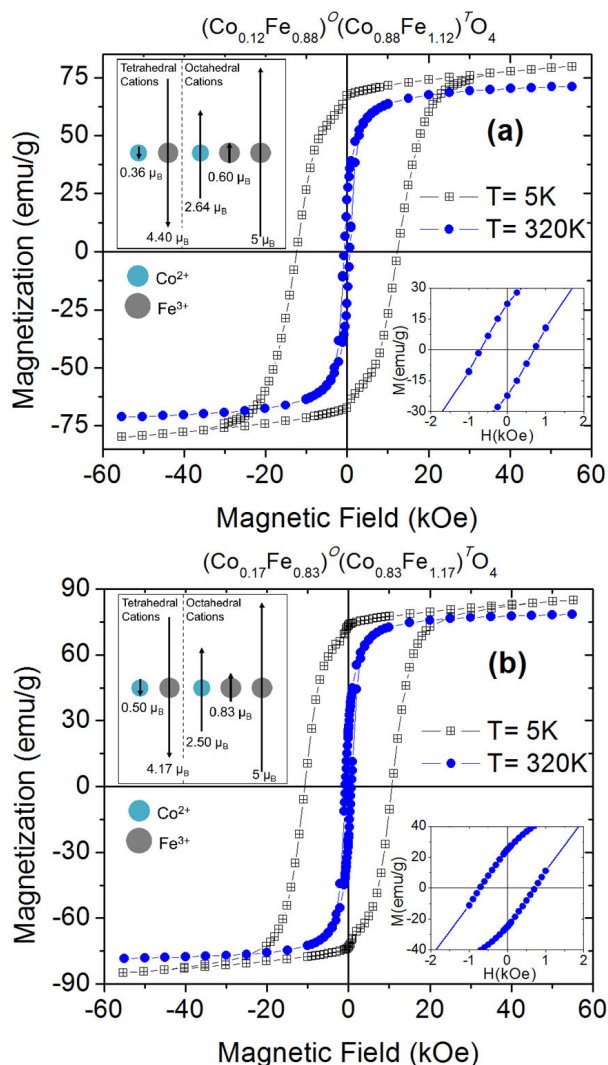


FIGURE 6. Magnetic field dependence of magnetization, at 5 and 320 K, of cobalt ferrite nanopowder samples calcined at (a) 873 K and (b) 1073 K. The upper insets show schematic representations of the magnetic ordering between the tetrahedral and octahedral cations in a formula unit of each nano-compound. The lower insets show  $M(H)$  curves at 320 K in the region of a small applied field.

of the blocking temperature, which suggests that in this nano-compound, most of the nanoparticles are in the blocked regime, even at room temperature.

The results discussed on  $ZFC - FC$  magnetization data, and the  $T_B$  distributions are consistent with the isothermal magnetization curves obtained at 5 and 320 K, shown in Fig. 6. The lower insets in this figure show  $M(H)$  curves at 320 K in the region of a small applied field. It is observed that all the magnetization curves exhibit hysteresis, without achieving saturation magnetization with the maximum applied magnetic field (5.5 T). The saturation magnetization ( $M_S$ ) values were determined from the relationship  $M = M_S(1 - \beta/H)$ , where  $\beta$  is a magnetic field-independent parameter, after extrapolating to infinite field the experimen-

tal data ( $M$  vs.  $1/H$ ) in the high field range. Table II shows the values of coercive field ( $H_C$ ), saturation magnetization,

TABLE II. Coercive field ( $H_C$ ), saturation magnetization ( $M_S$ ), and remanent magnetization ( $M_R$ ), measured at 5 and 320 K, of cobalt ferrite nanoparticles calcined at 873 and 1073 K.

Sample	$T_{\text{meas}}$ (K)	$H_C$ (Oe)	$M_S$	$M_R$
			(emu/g)	(emu/g)
Calcined at 873 K	5	12396	82.46	67.12
	320	703	73.17	22.32
Calcined at 1073 K	5	10690	87.33	73.20
	320	720	79.79	24.95

and remanent magnetization ( $M_R$ ) extracted from the  $M$  vs.  $H$  curves. The hysteresis loops at 5 K present extremely large coercive fields of approximately 12.4 and 10.7 kOe, for cobalt ferrite samples calcined at 873, and 1073 K, respectively. These  $H_C$  values are among the highest values reported for bulk and nanocrystalline cobalt ferrite [29]. For the sample calcined at 1073 K, the highest value of saturation magnetization was obtained,  $M_S = 87.33$  emu/g at 5 K. This value is very close to the bulk cobalt ferrite saturation magnetization value of 90 emu/g (at 0 K) [30]. The different saturation magnetization values obtained suggest that the  $\text{Co}^{2+}$  and  $\text{Fe}^{3+}$  cations are distributed differently in the two nano-compounds, generating variants in the internal magnetic structure of the nanoparticles. These results confirm that the magnetic properties of ferrites strongly depend on the cationic distribution between the tetrahedral and octahedral interstices of the spinel structure.

From the saturation magnetization values at 5 K, the inversion parameter ( $\lambda$ ) of the spinel structure was estimated for the two cobalt ferrite nano-compounds. The internal magnetic order of the nanoparticles in both samples, at low temperatures, must correspond to the ferrimagnetic arrangement, which is characteristic of bulk cubic ferrites [30]. Therefore, it was considered a collinear arrangement of the magnetic moments of the cations located in the tetrahedral and octahedral interstices of the spinel structure. Thus, the magnetic moment per formula unit ( $\mu_{f.u.}$ ) of the cobalt ferrite is  $\mu_{f.u.} = [\lambda \cdot \mu_{\text{Co}^o} + (2 - \lambda) \cdot \mu_{\text{Fe}}]^O - [(1 - \lambda) \cdot \mu_{\text{Co}} + \lambda \cdot \mu_{\text{Fe}}]^T$ , where  $\mu_{\text{Co}}$  is the spin-only magnetic moment of  $\text{Co}^{2+}$  ( $3 \mu_B$ ),  $\mu_{\text{Fe}}$  is the spin-only moment of  $\text{Fe}^{3+}$  ( $5 \mu_B$ ), O and T superscripts indicate the magnetic sublattices formed by the cations located in the octahedral and tetrahedral sites, respectively [30]. The values of  $\mu_{f.u.}$  corresponding to  $M_S$  (at 5 K) for the samples of  $\text{CoFe}_2\text{O}_4$  calcined at 873 and 1073 K are  $3.46 \mu_B$  and  $3.67 \mu_B$ , respectively. The inversion parameter values calculated are  $\lambda = 0.88$  for the ferrite calcined at 873 K and  $\lambda = 0.83$  for the sample calcined at 1073 K. Therefore, the formula unit of cobalt ferrite samples calcined at 873 and 1073 K can be written as  $(\text{Co}_{0.12}\text{Fe}_{0.88})^T(\text{Co}_{0.88}\text{Fe}_{1.12})^O\text{O}_4$  and  $(\text{Co}_{0.17}\text{Fe}_{0.83})^T(\text{Co}_{0.83}\text{Fe}_{1.17})^O\text{O}_4$ , respectively. The obtained  $\lambda$  values confirm that the cobalt ferrite crystallizes

in a partially inverse spinel structure, observing a reduction in the inversion degree with the increase in calcination temperature. The upper insets in Fig. 6 show graphical representations of the two collinear magnetic sublattices formed by the  $\text{Co}^{2+}$  and  $\text{Fe}^{3+}$  cations located in the tetrahedral and octahedral sites of the spinel structure; these magnetic arrangements generate magnetic moments per formula unit that are equivalent to the saturation magnetizations presented by the two nanopowders at 5 K. The results obtained confirm that the application of thermal treatments affects the cationic distribution in Co ferrite, which generates changes in the magnetic properties of the material.

#### 4. Conclusions

Cobalt ferrites in the form of nanoparticulate powders were synthesized by the coprecipitation method and subsequent thermal treatments. The mean particle sizes were 29 and 42 nm, for samples calcined, at 873 and 1073 K, respectively. The synthesized nanopowders have a single crystalline phase corresponding to the partially inverse spinel structure

with inversion parameters of 0.83 and 0.88. The temperature and magnetic field dependence of the magnetization revealed that both samples are formed by magnetic nanoparticles with strong interparticle interactions. The sample calcined at 873 K exhibits a superparamagnetic behavior at room temperature, with a considerable portion of nanoparticles in the blocked regime, while the particles of the sample calcined at 1073 K are mainly in the blocked regime, in the entire temperature range below 320 K. The magnetic properties exhibit some dependence on the calcination temperature:  $M_S$  and  $M_R$  values increase with the increase of calcination temperature. The  $M_S$  values are close to the saturation magnetization of the bulk cobalt ferrite. The maximum values of  $H_C$  are among the highest known values for  $\text{CoFe}_2\text{O}_4$ .

#### Acknowledgments

Authors are thankful to the Polymers Group of the Simón Bolívar University (USB) for their collaboration with the TEM images.

1. M. L. Néel, Propriétés magnétiques des ferrites; ferromagnétisme et antiferromagnétisme, *Ann. Phys.* **12** (1948) 137, <https://doi.org/10.1051/anphys/194812030137>.
2. J. Smit and H. P. J. Wijn, *Ferrites* (The Philips Technical Library, Eindhoven, 1959)
3. R. Valenzuela, Novel Applications of Ferrites, *Phys. Res. Int.* **2012** (2012) 591839, <https://doi.org/10.1155/2012/591839>.
4. S. Hazra and N. N. Ghosh, Preparation of nanoferrites and their applications, *J. Nanosci. Nanotechnol.* **14** (2014) 1983, <https://doi.org/10.1166/jnn.2014.8745>.
5. V. G. Harris *et al.*, Recent advances in processing and applications of microwave ferrites, *J. Magn. Magn. Mater.* **321** (2009) 2035, <https://doi.org/10.1016/j.jmmm.2009.01.004>.
6. I. Sharifi, H. Shokrollahi, and S. Amiri, Ferrite-based magnetic nanofluids used in hyperthermia applications, *J. Magn. Magn. Mater.* **324** (2012) 903, <https://doi.org/10.1016/j.jmmm.2011.10.017>.
7. D. S. Mathew and R.-S. Juang, An overview of the structure and magnetism of spinel ferrite nanoparticles and their synthesis in microemulsions, *Chem. Eng. J.* **129** (2007) 51, <https://doi.org/10.1016/j.cej.2006.11.001>.
8. S. Amiri and H. Shokrollahi, The role of cobalt ferrite magnetic nanoparticles in medical science, *Mater. Sci. Eng. C* **33** (2013) 1, <https://doi.org/10.1016/j.msec.2012.09.003>.
9. T. A. S. Ferreira *et al.*, Structural and morphological characterization of  $\text{FeCo}_2\text{O}_4$  and  $\text{CoFe}_2\text{O}_4$  spinels prepared by coprecipitation method, *Solid State Sci.* **5** (2003) 383, [https://doi.org/10.1016/S1293-2558\(03\)00011-6](https://doi.org/10.1016/S1293-2558(03)00011-6).
10. S. D. Bhamé and P. A. Joy, Enhanced magnetostrictive properties of  $\text{CoFe}_2\text{O}_4$  synthesized by an autocombustion method, *Sens. Actuators A* **137** (2007) 256, <https://doi.org/10.1016/j.sna.2007.03.016>.
11. I. H. Gul, A. Maqsood, M. Naeem, and M. Naeem Ashiq, Optical, magnetic and electrical investigation of cobalt ferrite nanoparticles synthesized by co-precipitation route, *J. Alloys Compd.* **507** (2010) 201, <https://doi.org/10.1016/j.jallcom.2010.07.155>.
12. J. Wang, T. Deng, Y. Lin, C. Yang, and W. Zhan, Synthesis and characterization of  $\text{CoFe}_2\text{O}_4$  magnetic particles prepared by co-precipitation method: Effect of mixture procedures of initial solution, *J. Alloys Compd.* **450** (2008) 532, <https://doi.org/10.1016/j.jallcom.2007.02.099>.
13. C. Jaimes, E. Santiago, V. Sagredo, and G. Márquez, Síntesis y caracterización de nanopartículas de ferrita de cobalto, *Rev. Cienc. Ing.* **40** (2019) 165, <http://erevistas.saber.ula.ve/index.php/cienciaeingenieria>.
14. M. Mozaffari, J. Amighian, and E. Darsheshdar, Magnetic and structural studies of nickel-substituted cobalt ferrite nanoparticles, synthesized by the sol-gel method, *J. Magn. Magn. Mater.* **350** (2014) 19, <https://doi.org/10.1016/j.jmmm.2013.08.008>.
15. P. C. R. Varma *et al.*, Magnetic properties of  $\text{CoFe}_2\text{O}_4$  synthesized by solid state, citrate precursor and polymerized complex methods: A comparative study, *J. Alloys Compd.* **453** (2008) 298, <https://doi.org/10.1016/j.jallcom.2006.11.058>.
16. A. B. Salunkhe, V. M. Khot, M. R. Phadatore, and S. H. Pawar, Combustion synthesis of cobalt ferrite nanoparticles-Influence of fuel to oxidizer ratio, *J. Alloys Compd.* **514** (2012)

- 91, <https://doi.org/10.1016/j.jallcom.2011.10.094>.
17. G. Márquez and V. Sagredo, Síntesis y caracterización de nanocompuestos de CoM<sub>2</sub>O<sub>4</sub> (M = Cr, Fe), *Ciencia* **19** (2011) 277, <https://produccioncientificaluz.org/index.php/ciencia>.
  18. M. J. Iqbal and M. R. Siddiquah, Electrical and magnetic properties of chromium-substituted cobalt ferrite nanomaterials, *J. Alloys Compd.* **453** (2008) 514, <https://doi.org/10.1016/j.jallcom.2007.06.105>.
  19. W. S. Chiu, S. Radiman, R. Abd-Shukor, M. H. Abdullah, and P. S. Khiew, Tunable coercivity of CoFe<sub>2</sub>O<sub>4</sub> nanoparticles via thermal annealing treatment, *J. Alloys Compd.* **459** (2008) 291, <https://doi.org/10.1016/j.jallcom.2007.04.215>.
  20. S. Gyergyek *et al.*, Influence of synthesis method on structural and magnetic properties of cobalt ferrite nanoparticles, *J. Nanopart. Res.* **12** (2010) 1263, <https://doi.org/10.1007/s11051-009-9833-5>.
  21. E. Swatsitang *et al.*, Characterization and magnetic properties of cobalt ferrite nanoparticles, *J. Alloys Compd.* **664** (2016) 792, <https://doi.org/10.1016/j.jallcom.2015.12.230>.
  22. F. Morales, G. Márquez, V. Sagredo, T. E. Torres, and J. C. Denardin, Structural and magnetic properties of silica-coated magnetite nanoaggregates, *Physica B* **572** (2019) 214, <https://doi.org/10.1016/j.physb.2019.08.007>.
  23. J. B. Silva, W. de Brito, and N. D. S. Mohallem, Influence of heat treatment on cobalt ferrite ceramic powders, *Mat. Sci. Eng. B* **112** (2004) 182, <https://doi.org/10.1016/j.mseb.2004.05.029>.
  24. E. Pérez, G. Márquez, and V. Sagredo, Effect of Calcination on Characteristics of Nickel Ferrite Nanoparticles Synthesized by Sol-Gel Method, *Iraqi J. Appl. Phys.* **15** (2019) 13, <https://www.iasj.net/iasj?func=issues&jId=262>.
  25. S. E. Shirsath, B. G. Toksha, and K. M. Jadhav, Structural and magnetic properties of In<sup>3+</sup> substituted NiFe<sub>2</sub>O<sub>4</sub>, *Mat. Chem. Phys.* **117** (2009) 163, <https://doi.org/10.1016/j.matchemphys.2009.05.027>.
  26. R. D. Waldron, Infrared Spectra of Ferrites, *Phys. Rev.* **99** (1955) 1727, <https://doi.org/10.1103/PhysRev.99.1727>.
  27. A. A. Ati, Z. Othaman, and A. Samavati, Influence of cobalt on structural and magnetic properties of nickel ferrite nanoparticles, *J. Mol. Struct.* **1052** (2013) 177, <https://doi.org/10.1016/j.molstruc.2013.08.040>.
  28. D. Peddis, C. Cannas, A. Musinu, and G. Piccaluga, Magnetism in Nanoparticles: Beyond the Effect of Particle Size, *Chem. Eur. J.* **15** (2009) 7822, <https://doi.org/10.1002/chem.200802513>.
  29. T. Meron, Y. Rosenberg, Y. Lereah, and G. Markovich, Synthesis and assembly of high-quality cobalt ferrite nanocrystals prepared by a modified sol-gel technique, *J. Magn. Magn. Mater.* **292** (2005) 11, <https://doi.org/10.1016/j.jmmm.2004.10.084>.
  30. B. D. Cullity and C. D. Graham, *Introduction to Magnetic Materials*, 2nd ed. (IEEE Press, New York, 2009).